Corrosion Science 76 (2013) 42–51

Contents lists available at SciVerse ScienceDirect

Corrosion Science

journal homepage: www.elsevier.com/locate/corsci

Surface characterization and corrosion behavior of a novel gold-imitation copper alloy with high tarnish resistance in salt spray environment

Zhu Xiao [a,b], Zhou Li [a,c,*], Anyin Zhu [a,d], Yuyuan Zhao [b], Jinglin Chen [a,d], Yuntian Zhu [a]

[a] School of Materials Science and Engineering, Central South University, Changsha 410083, China
[b] School of Engineering, University of Liverpool, Liverpool L69 3GH, UK
[c] State Key Laboratory of Powder Metallurgy, Changsha 410083, China
[d] Key Laboratory of Nonferrous Metal Materials Science and Engineering, Ministry of Education, Changsha 410083, China

ARTICLE INFO

Article history:
Received 28 December 2012
Accepted 29 May 2013
Available online 2 July 2013

Keywords:
A. Alloy
B. Polarization
B. EIS
B. XPS
C. De-alloying
C. Passive films

ABSTRACT

A novel gold-imitation copper alloy (CuZnAlNiSnBRe) was designed and its corrosion behavior in salt spray environment was investigated. The new alloy has better tarnish resistance and corrosion resistance than the current coinage alloy used in China (H7211). A multi-layer film formed on the surface of the new alloy after a period of exposure to salt spray was responsible for the good resistance of the alloy. The corrosion products were a mixture of CuO, Cu_2O, ZnO, Al_2O_3 and $Al(OH)_3$, with the transition from Cu_2O to CuO occurring during the corrosion process.

1. Introduction

Copper-based alloys are widely used in many industries [1–3]. One of the applications is for manufacturing coins and medals. Many copper-based alloys, such as Cu–Zn [4,5], Cu–Al [6] and Cu–Ni [7], have been developed as mintage and ornamental materials, due to their nobility, various beautiful colors, remarkable cast ability and good formability [4–9]. Table 1 lists a selection of the mintage of a few countries made from copper-based alloys [10].

The color of gold is often preferred for mintage or commemorative coins. Zinc, which is a key component of brass, is considered as the best element to increase the brightness of the golden color of gold-imitation copper alloys. However, dezincification in brass is a common problem. The alloy develops a reddish color with de-alloying, which contrasts with its original yellowish color and can be readily observed with naked eyes [11]. Generally, there are two types of de-alloying, depending on the zinc content. For alloys with high zinc content, uniform or layer de-alloying commonly occurs, with the outer layer showing a dark color. For alloys with low zinc content, plug de-alloying occurs, typified by the presence of the de-alloyed dark plugs in the otherwise unaffected matrix [2,11–13].

In the present work, a new aluminum (Al) brass alloy with 24 k-gold color was designed and prepared. The corrosion behavior of the new alloy was studied by salt spray test and polarization curve characterization. X-ray photoelectron spectroscopy (XPS), which can provide more comprehensive and accurate information of the surface than X-ray diffraction (XRD) and energy dispersive spectroscopy (EDX), was employed to characterize the nature and the composition of the corrosion product layer on the surface as a function of exposure time. Electrochemical impedance spectroscopy (EIS) was used to obtain further insights into the mechanisms of the accelerated attack of the alloy in the corrosive environment.

2. Experimental procedures

2.1. Alloy preparation

A new gold-imitation alloy with 24 k-gold color was prepared by induction melting and mold casting. The new alloy was designed with additions of Al and rare earth and its composition is shown in Table 2. The surface defects of the ingot were first removed by mechanical milling. The ingot was then homogenized at 1023 K for 2 h and subsequently hot-rolled from a thickness of 22–4 mm, and then cold-rolled to 2 mm. The as-produced strip was annealed at 963 K for 1 h. As a comparison, the H7211 copper alloy (a currency coinage alloy with 24 k-gold color) provided by Shenyang Mint, China, was also tested.

* Corresponding author at: School of Materials Science and Engineering, Central South University, Changsha 410083, China. Tel.: +86 73188830264; fax: +86 73188876692.
E-mail address: lizhou6931@163.com (Z. Li).

0010-938X/$ - see front matter © 2013 Elsevier Ltd. All rights reserved.
http://dx.doi.org/10.1016/j.corsci.2013.05.026

Table 1
Selected mintage alloys [10].

Currency	Denomination	Materials
UK pound	1-Penny, 2-pence	Copper-plated steel
	5-, 10-, 50-pence and £5	B25
	20-pence	B16
	£1	HNi70–5.5
	£2	HNi76–4 (outer), B25 (inner)
Euro	10-, 20- and 50-cent	CuAl5Zn5Sn1
	€1	CuZn20Ni (outer), B25/7%Ni/B25 (inner)
	€2	B25 (outer), CuZn20Ni5/12%Ni/CuZn20Ni5 (inner)
US dollar	1-cent	Copper-plated zinc
	2-cent	Nickel-brass
	10-, 25- and 50-cent	B25-plated B17
	$ 1	Copper with manganese brass clad
Australian Dollar	5-, 10-, 20- and 50-cent	B25
	$ 1 and $ 2	Cu92Al6Ni2
Chinese Yuan	50-cent	H7211
Commemorative coin made by Poongan Co.		B25,Cu89Zn5Al5Sn1,H65,HNi70–12,HNi75–5

2.2. Salt spray test and color difference measurement

The salt spray test was carried out in a LYW-025 salt spray test chamber with 5% sodium chloride solution at a constant temperature of 35 °C. The specimens with dimensions of 10 mm × 10 mm × 2 mm were first cut from the strips of the two alloys with a high speed cutting machine. The surfaces of the specimens were ground carefully using 1200 grit paper and polished. The specimens were subsequently dehydrated by 90% ethanol for 5 min and then dried by hot air for testing. A group of specimens were exposed in the salt spray environment for different times up to 240 h. The color differences between the specimens after different exposure times and gold were measured by a CC-6801 colorimeter (BYK, German) to investigate the tarnish resistance of the alloys.

The color difference, ΔE, was calculated according to the CIE1976LAB standard:

$$\Delta E = \sqrt{(L_t - L_g)^2 + (a_t - a_g)^2 + (b_t - b_g)^2} \quad (1)$$

where L is lightness, a is red–green opponent, and b is yellow–blue opponent; the subscript t designates the tested sample, and g the calibrating sample, i.e. gold (L_g = 36.97, a_g = 5.22, b_g = 24.04).

2.3. Electrochemical test

Electrochemical characterization was carried out on an IM6ex electrochemical workstation using Pt as the auxiliary electrode and the saturated calomel electrode (SCE) as the reference electrode. The surface of each specimen for the electrochemical test was sealed with paraffin, except an uncovered area of 1 cm^2. The specimens were exposed in salt spray environment for 6 h, 12 h, 24 h, 60 h, 120 h and 240 h and then tested. All electrochemical measurements were performed after the open circuit potential (OCP) was stabilized. The potentiodynamic polarization measurements were performed by scanning from −200 mV (SCE) to 600 mV (SCE) with a speed of 2 mV/s and the data were analyzed by the CHI660C software. In the EIS measurements, the AC voltage signal amplitude was 10 mV (peak to zero), the frequency was between 100 kHz and 10 mHz, and 101 points were measured. The experimental data were analyzed by the Zview software.

Table 2
Composition of the new alloy.

Alloy elements	Cu	Al	Ni	Sn	B	Re	Zn
Content (wt.%)	76	2	0.5	0.2	0.01	0.05	Balance

2.4. X-ray photoelectron spectroscopy (XPS) analysis

The XPS analysis of the specimens of the new alloy after exposed in salt spray environment for 6 h and 60 h was performed on a K-Alpha 1063 X-ray photoelectron spectroscope (Thermo Fisher Scientific), with a monochromotized Al Kα X-ray source in vacuum of 10^{-9} mBar. The spot diameter was 400 μm and the step lengths were 1 eV for wide scanning and 0.1 eV for narrow scanning. The output of the analysis was recorded as binding energy vs. intensity count plots through a data logger system. The specimens were immersed in deionized water for 5 min and then dried in vacuum drying oven for 15 min before testing. The high resolution photoelectron spectra were recorded for Cu2p, Zn2p, Al2p and O1s. The data reduction was performed by deconvoluting the high resolution composite XPS peaks of the individual species having different oxidation states using the XPSPEAK software based on a non-linear least square regression method. The peak position and peak width (FWHW) of the individual species obtained from Ref. [14] were used as input parameters in deconvoluting the spectra. The criteria for the best fit were judged by the smallest Chi-Square value. The final results consisted of the area under each of the resolved peaks for the individual oxidation states, the total area under raw data and the total area under the convoluted curves.

2.5. Microstructure analysis by SEM

The samples of the new alloy exposed in salt spray environment for 6 h and 60 h were rinsed with deionized water for three times and then air dried. The morphology and the thickness of the corrosion layer were observed and analyzed using a Siron200 Scanning Electron Microscope (FEI Co., Holland).

3. Results and discussion

3.1. Tarnish resistance

Fig. 1 shows the variations of the color difference of the new alloy and the H7211 alloy after being exposed in salt spray environment for different times. For both alloys, the color difference increased rapidly with exposure time for the first 60 h. After the 60 h exposure, the color difference of the H7211 alloy became stable while that of the new alloy continued to increase, but with a

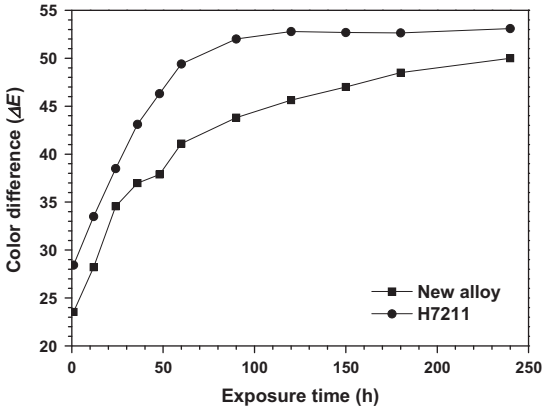

Fig. 1. Color difference of the new alloy and the H7211 alloy after being exposed in the salt spray environment for different times.

much slower rate. However, the color difference of the new alloy was always less than that of the H7211 alloy for every exposure time. The better tarnish resistance of the new alloy may be attributed to the addition of Al, Sn and rare earth, which could form a thin, dense and well-bonded surface layer, preventing further corrosion in the alloy in salt spray environment.

The corrosion rate of copper alloys in salt environments normally follows the power law [15]. The relationship between the color difference ($\triangle E$) and corrosion time (t) may be expected to obey the power law, i.e.:

$$\Delta E = At^n \text{ or } \log(\Delta E) = n\log t + \log A \quad (2)$$

where A and n are constants related to the alloy and the corrosive environment.

Fig. 2 plots the color difference vs. exposure time data in logarithmic scales for both alloys. The logarithmic Eq. (2) fits well for the new alloy for exposure times up to 180 h and for the H7211 alloy up to 60 h (with squared correlation coefficients, r^2, of 0.99), confirming the applicability of the power law relationship to color difference in the early stage of corrosion. The new alloy has lower A and n values (16.6, 0.21) than the H7211 alloy (18.2, 0.24), confirming that the former has better tarnish resistance than the latter in salt spray environment.

3.2. Polarization curve measurements

Fig. 3 shows the polarization curves of the two alloys after being exposed in salt spray environment for different times. It can be seen that the corrosion potentials of both alloys shift to the positive direction (about 110 mV for the new alloy and 75 mV for the H7211 alloy) after exposure in salt spray environment for 240 h, which can possibly be interpreted by the inhibitive effect on the anodic reaction of the protective oxide film in terms of the mixed potential theory [16]. The polarization resistance was calculated by:

$$R_p = \frac{b_a \times b_c}{2.3(b_c - b_a) \times i_{corr}} \quad (3)$$

Table 3 summarizes the characteristic parameters of the electrochemical test: anode Tafel slope b_a, cathode Tafel slope b_c, corrosion current density i_{corr}, corrosion potential E_{corr} and polarization resistance R_p. It shows b_a and b_c seem to be independent exposure time in salt spray environment, which was also found in studying the cathodic and anodic polarization characteristics of the 70/30 Cu–Ni alloy in aerated sulfide-containing simulated seawater [17]. Table 3 also shows that the polarization resistance increases, and the corrosion current decreases with increasing the exposure time in salt spray environment. The polarization resistance of the new alloy is more than three times of that of the H7211 alloy, showing that the former has much better corrosion resistance than the latter.

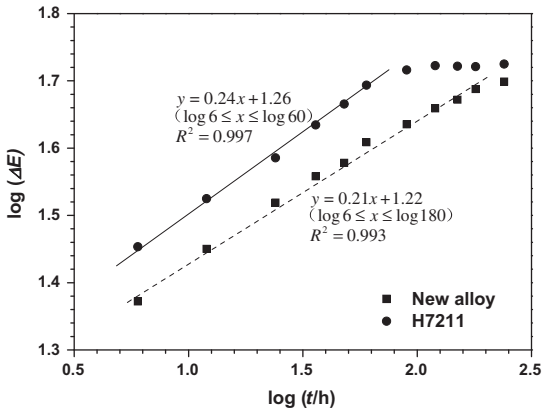

Fig. 2. Relationship between color difference and exposure time in salt spray for the new and H7211 alloys.

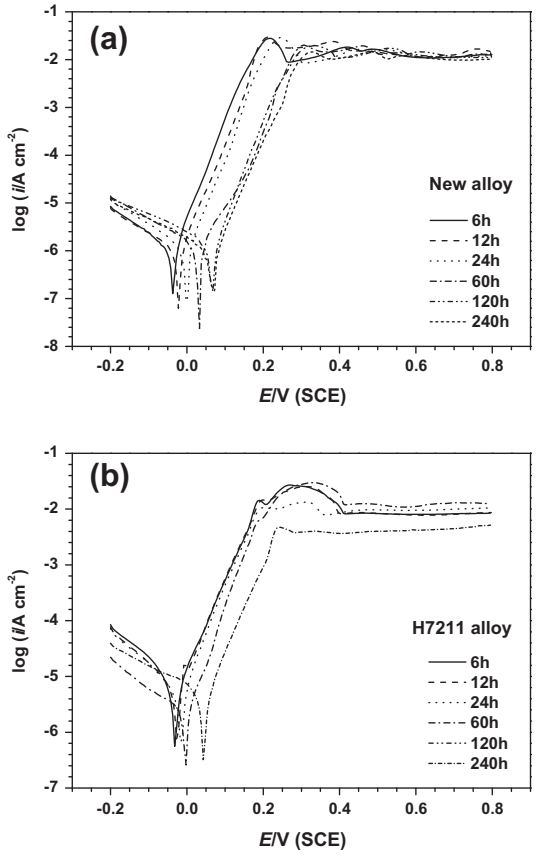

Fig. 3. The polarization curves of (a) the new alloy and (b) the H7211 alloy after exposed in salt spray environment for different times.

3.3. Impedance measurements

Fig. 4 shows the impedance spectra of the samples of the new alloy after being exposed in salt spray environment for different times. The Nyquist spectra in Fig. 4a have roughly semicircle shapes and the diameter of the semicircle increases with frequency, suggesting that the charge transfer resistance of the oxide

Table 3
Characteristic parameters obtained from the polarization curves of the two alloys after being exposed in salt spray environment for different times.

Alloy	Exposure time (h)	b_a (mV/Dec)	b_c (mV/Dec)	E_{corr} (V)	I_{corr} ($\times 10^{-6}$ A/cm^2)	R_p ($\times 10^3$ Ω cm^2)
New alloy	6	49.8	−202.7	−0.037	2.051	8.474
	12	50.1	−198.2	−0.022	1.521	11.432
	24	46.4	−208.9	−0.017	1.347	12.255
	60	50.5	−223.9	0.033	1.298	13.803
	120	53.2	−285.0	0.068	1.119	17.419
	240	53.3	−276.0	0.073	1.014	19.155
H7211	6	61	−196.5	−0.032	7.133	2.837
	12	64.6	−210.5	−0.027	7.019	3.062
	24	63.8	−228.6	−0.017	5.436	3.989
	60	60.3	−195.1	−0.002	4.610	4.344
	120	51.1	−206.5	0.023	3.934	4.527
	240	53.6	−239.9	0.043	3.170	6.009

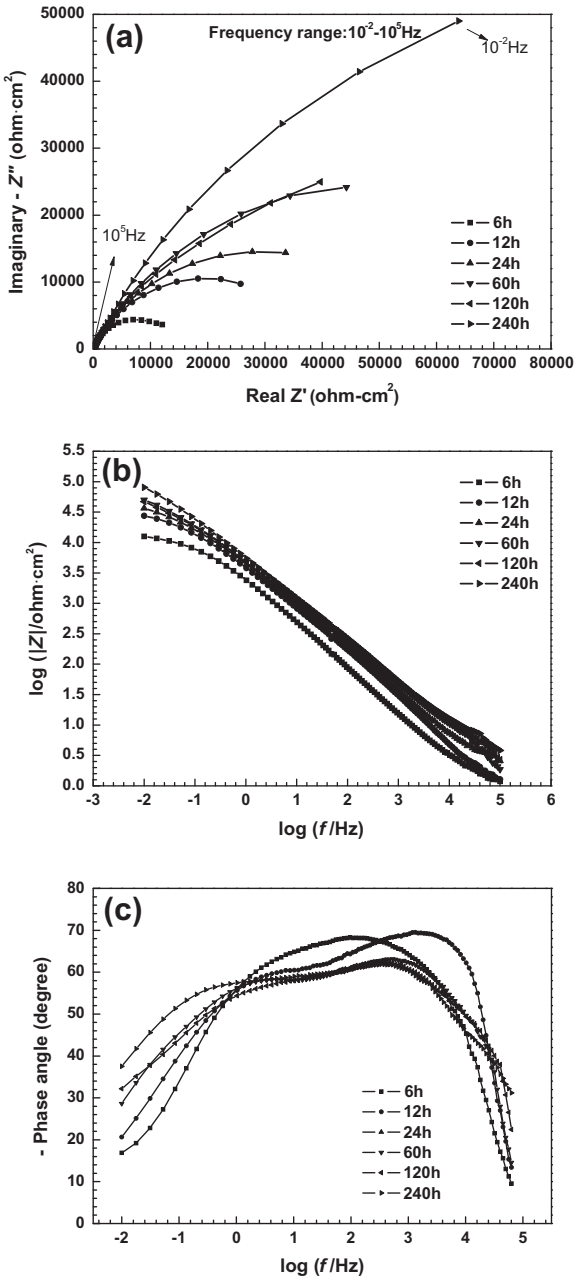

Fig. 4. Impedance spectra of the new alloy after being exposed in salt spray environment for different times: (a) Nyquist spectra, (b) Bode spectra – impedance and (c) Bode spectra – phase angle.

film increases with exposure time. The Bode spectra in Fig. 4b shows that the impedance generally increases with exposure time over all frequencies (at 10^{-2} Hz, for example, log $|Z|$ increases from 4.1 to 4.9 when the exposure time is increased from 6 h to 240 h), indicating the growth of the protective oxide film. In the medium frequency region ($10^{-0.5}$ to $10^{4.5}$), the relationship between log $|Z|$ and log f is nearly linear with a slope close to −1. This capacitive behavior may be related to the electrical double layer (EDL) at the solution/metal interface, the corrosion product film/metal surface, or both. However, the capacitive behavior normally disappears at low frequency, showing that diffusion process starts to play an important role [18]. The phase angle Bode plots in Fig. 4c shows that two peaks appear at the low and high frequency regions after 12 h of exposure. This can be attributed to the formation of a multi-layer protective corrosion product film [17,19]. The peak angle in the low frequency region is related to EDL. It increases gradually with exposing time, indicating a decrease in the corrosion rate of the alloy with time [17]. The peak angle in the high frequency region generally decreases with exposure time, from approximately 69.5° to 61.9° from 12 h to 240 h.

Table 4 shows four physical models and their corresponding equivalent circuits used to fit the impedance data of the new alloy after being exposed in salt spray environment. The symbols in the equivalent circuits are: R_s – solution resistance; C_{film} – capacitance of the corrosion product film; R_{film} – resistance of the corrosion product film; R_{ct} – charge transfer resistance; CPE – constant phase element, which is a capacitive description of the EDL at the corrosion product/metal interface; W_s – finite length diffusion (or finite Warburg) element, producing a finite Warburg impedance, Z_w.

The impedance of CPE, Z, can be obtained by [18]:

$$\frac{1}{Z} = Q_0(j\omega)^{n_1} \tag{4}$$

where Q_0 is the admittance (the inverse of impedance $1/|Z|$) at $\omega = 1$ rad/s, j is the imaginary number ($j^2 = -1$), ω is angular frequency ($\omega = 2\pi f$) and n_1 is the CPE exponent. CPE represents an idealized capacitance, which can be taken as a resistance for $n_1 = 1$, an inductance for $n1 = -1$ and a Warburg impedance for $n1 = 0.5$ [20].

The Warburg element, W_s, could be attributed to a diffusion process taking place in the solid phase. If the surface layer is thin, low frequencies will penetrate the entire thickness, creating a Finite-Length-Warburg (FLW) element [21]:

$$Z_W = \frac{W_R \tanh(j\omega T)^{n_2}}{(j\omega T)^{n_2}} \tag{5}$$

where W_R is associated with solid phase diffusion, n_2 is the FLW exponent and T is related to the effective diffusion coefficient (D) and the effective diffusion thickness (L) by $T = L^2/D$. Only if the material is thick enough so that the lowest frequencies do not penetrate the entire layer, it can be interpreted as infinite diffusion.

Table 4
Physical models and corresponding equivalent circuits used to fit the impedance data of the new alloy after being exposed in salt spray environment.

No.	Physical models	Equivalent circuits	χ^2
I	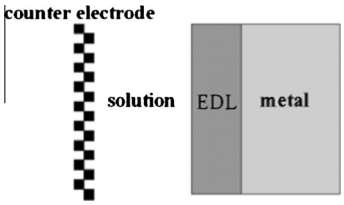	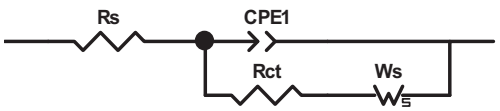	0.021
II	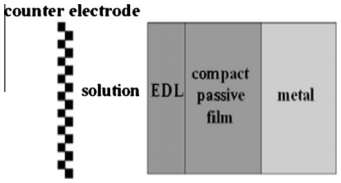	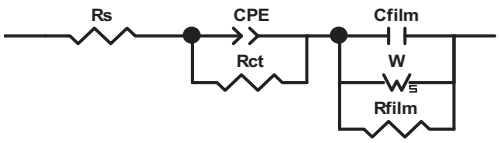	0.003
III	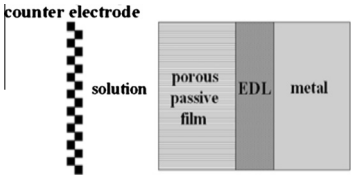	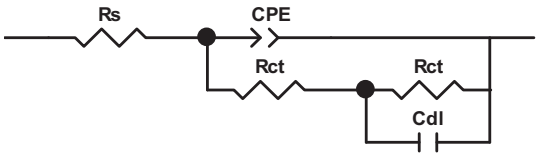	0.005
IV	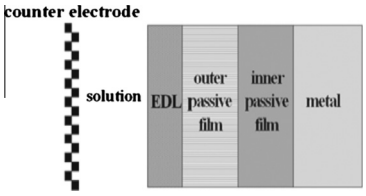	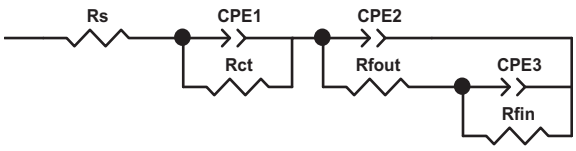	0.016

Ignoring the solution resistance, the resistance of the equivalent circuit, R, can be calculated by:

$$R = R_{ct} + \frac{W_R \cdot R_{film}}{W_R + R_{film}} \tag{6}$$

The goodness of fit parameter χ^2 for each of the four models was calculated by the following equation [22]:

$$\chi^2 = \sum_{i=1}^{N} \frac{[Z_i' - Z'(\omega_i)]^2 + [Z_i'' - Z''(\omega_i)]^2}{\sigma^2} \tag{7}$$

where N is the number of data points, Z_i' and Z_i'' are the measured real and imaginary impedances, $Z'(\omega_i)$ and $Z''(\omega_i)$ are the calculated real and imaginary impedances from the model, and σ^2 is the variance of the measured data. The χ^2 values for the equivalent circuits are given in Table 4. It shows that Model II has the lowest χ^2 value and fits best with the measured EIS data. Therefore, Model II (metal/passive film/EDL) is considered the most appropriate model.

Table 5 shows the impedance parameters of the new alloy after being exposed in salt spray environment for different times, obtained using Model II (see Table 4 for the equivalent circuit). The capacitance of the corrosion product film, C_{film}, decreases and the resistance, R_{film}, increases with exposure time, indicating the growth of the film [18,23]. The coefficient of CPE, Q_0, decreases with exposure time while n increases with exposure time, indicating that the film is getting thicker and denser [23]. The transfer resistance, R_{ct}, Warburg impedance, W_R, and the equivalent circuit resistance, R_0, increase with exposure time (especially in the first 60 h), indicating that the resistance to the corrosion process increases and the corrosion rate decreases.

3.4. XPS analysis of the corrosion product layer

XPS analysis was undertaken for two samples of the new alloy after having been exposed in the salt spray chamber for 6 h and 60 h, respectively, and the wide XPS spectra are shown in Fig. 5. It can be seen that the main elements in the corrosion product layer are Cu, Al, Zn, O and Cl. Ni, Sn, B and Re were not detected due to their low concentrations in the alloy.

3.4.1. Cu2p spectra

Fig. 6 shows the Cu2p3/2 spectra of the corrosion product layer on the surface of the new alloy samples exposed in salt spray environment for 6 h and 60 h, respectively. The core-level spectrum was recorded in the range of 928–938 eV, and a peak appeared at 932.5 eV in the high resolution Cu2p3/2 spectra. The peaks of metallic Cu, and Cu_2O are difficult to distinguish due to the small

Table 5
Elements of the equivalent circuit for the new alloy after being exposed in salt spray environment for different times.

Exposing time (h)	R_s (Ω cm^2)	$10^6 \times Q_0$ (Ω^{-1} cm^{-2} s^n)	n_1	R_{ct} (Ω cm^2)	W_R (Ω cm^2)	T	n_2	C_{film} (μF/cm^2)	R_{film} (Ω cm^2)	R (Ω cm^2)
6	1.50	256.92	0.65	2376	145,13	3.682	0.53	20.36	3255	5035
12	1.91	85.76	0.71	3411	17,100	20.49	0.56	11.71	5242	7423
24	2.00	17.16	0.74	6226	29,800	29.48	0.48	7.97	6218	11,370
60	1.63	10.04	0.88	10,875	49,579	110.30	0.47	5.90	11,005	19,881
120	1.66	8.88	0.91	12,949	66,731	263.00	0.55	3.78	13,427	24,127
240	1.89	3.85	0.95	14,761	72,289	329.30	0.47	2.48	16,820	28,405

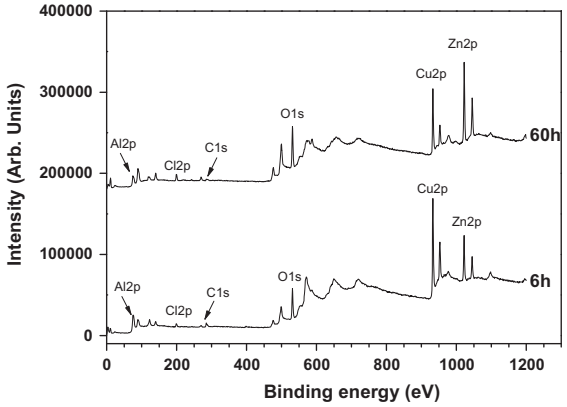

Fig. 5. Wide XPS spectra for the surface of the samples exposed in salt spray environment for 6 h and 60 h, respectively.

difference in binding energy between them, so they are expressed as Cu/Cu_2O. The corrosion products for the sample exposed for 6 h contained mainly Cu/Cu_2O (85.5%) and a small amount of CuO (14.5%) (Fig. 6a). With a prolonged exposure time of 60 h, the concentration of CuO increased significantly (Fig. 6b), about twice as much as in the sample with an exposure time of 6 h. The results are in accordance with literature [17,19] and indicate that the corrosion layer consists of an inner Cu_2O layer and an outer CuO layer. It is safe to speculate that a transition of corrosion product from Cu_2O to CuO occurs during the long-time corrosion in the salt spray environment. However, CuCl and $Cu_2(OH)_3Cl$, which commonly appear in the corrosive layer [17,24], is not found in the present study.

3.4.2. Zn2p spectra

Fig. 7 shows the Zn2p spectra of the corrosion product layer on the surface of the samples. The peak at 1021.6 eV belongs to Zn and the other small peak at 1022.3 eV can be attributed to ZnO. The concentration of ZnO in the corrosion product layer increased from 12.2% to 18.2% when the exposure time was increased from 6 h to 60 h.

3.4.3. Al2p spectra

Fig. 8 shows the Al2p spectra of the corrosion product layer on the surface of the samples. Al mainly exists in the form of Al_2O_3 and $Al(OH)_3$, the latter of which can be dissolved during the corrosion process. The two peaks at 74.2 eV and 74.7 eV are attributable to $Al(OH)_3$ and Al_2O_3, respectively. Al_2O_3 formed at the early stage of corrosion in the salt spray environment and its concentration increased from 73.9% to 81.7% when the exposure time was increased from 6 h to 60 h. The spectra also show a wide peak from 75 eV to 77.5 eV, which should be referred to the Cu3p spectra and are caused by Cu and its corrosion products.

3.4.4. O1s spectra

Fig. 9 shows the core-level O1s spectra of the corrosion product layer on the surface of the samples. To correlate with the Cu2p, Zn2p and Al2p spectra and to certify the existence of certain species, the O1s spectrum was deconvoluted into the corresponding components and combined with the above three spectra. Fig. 9 shows that the sample exposed for 6 h had a high concentration of Cu_2O and low concentration of CuO, while the sample exposed for 60 h had decreased Cu_2O and increased CuO concentrations. Al_2O_3 and ZnO also increased significantly with exposure time. These results are in good agreement with those obtained from the Cu2p, Zn2p and Al2p spectra.

3.4.5. Discussion on the corrosion process

The current XPS study showed that the main corrosion products of the new alloy exposed in salt spray environment were CuO, Cu_2O, ZnO, Al_2O_3 and $Al(OH)_3$. No chlorides were found from the XPS analysis, probably because of their low concentrations in the corrosion layer. However, chlorine ion is expected to play an important role in the corrosion process.

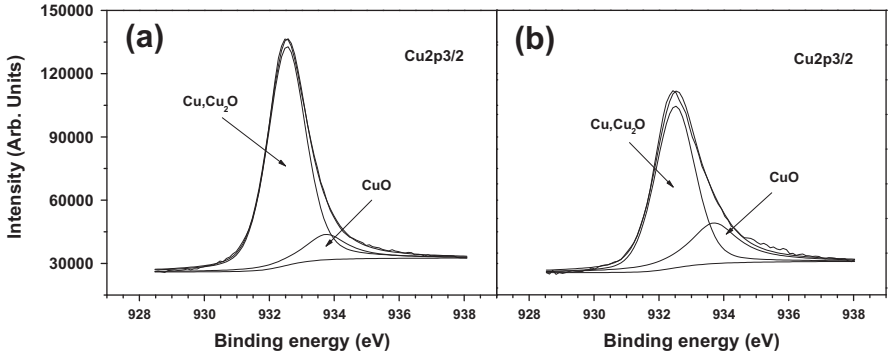

(c)

Valence state	*Exposure time (h)*	Proposed compounds	*Binding energy (eV)*	*Intensity area*	*Relative quantity*	$\Sigma\chi^2$
Cu2p3/2	6	Cu/ Cu_2O	932.5	176910.4	0.855	1.18
		CuO	933.7	29975.6	0.145	1.18
	60	Cu/ Cu_2O	932. 5	104661.9	0.709	1.23
		CuO	933.21	43040.4	0.291	1.23

Fig. 6. Cu XPS spectra and fitted parameters of the corrosion product layer of the samples exposed in salt spray environment for different times: (a) 6 h, (b) 60 h, and (c) fitting parameters for Cu XPS spectra and relative quantity of compounds.

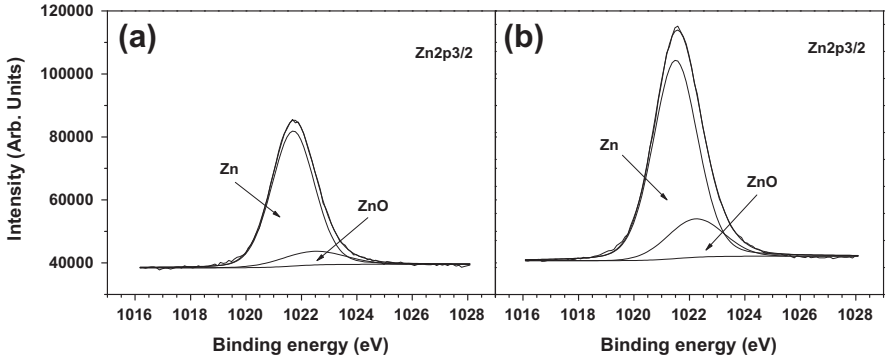

(c)

Valence state	*Exposure time (h)*	Proposed compounds	*Binding energy (eV)*	*Intensity area*	*Relative quantity*	$\Sigma\chi^2$
Zn2p3/2	6	Zn	1021.7	88128.34	0.878	0.89
		ZnO	1022.5	12281.39	0.122	0.89
	60	Zn	1021.6	160182.1	0.818	0.94
		ZnO	1022.3	35636.51	0.182	0.94

Fig. 7. Zn XPS spectra and fitted parameters of the corrosion product layer of the samples exposed in salt spray environment for different times: (a) 6 h, (b) 60 h, and (c) fitting parameters for Zn XPS spectra and relative quantity of compounds..

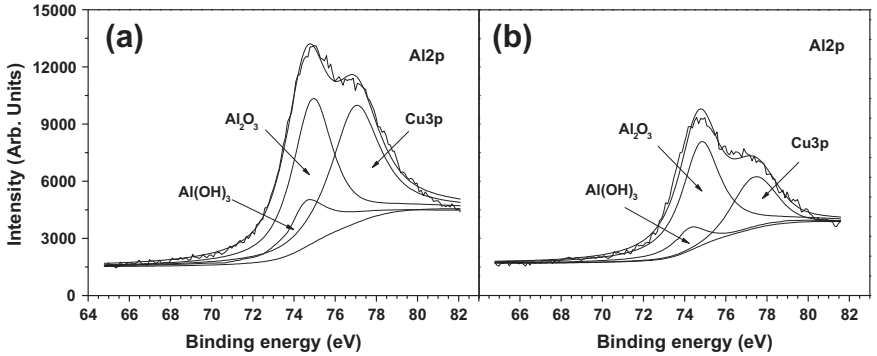

(c)

Valence state	*Exposure time (h)*	Proposed compounds	*Binding energy (eV)*	*Intensity area*	*Relative quantity*	$\Sigma\chi^2$
Al2p3/2	6	$Al(OH)_3$	74.2	5809.92	0.261	1.26
		Al_2O_3	74.7	18749.25	0.739	1.26
	60	$Al(OH)_3$	74.2	3029.47	0.183	1.14
		Al_2O_3	74.7	13524.96	0.817	1.14

Fig. 8. Al XPS spectra and fitted parameters of the corrosion product layer of the samples exposed in salt spray environment for different times: (a) 6 h, (b) 60 h, and (c) fitting parameters for Al XPS spectra and relative quantity of compounds.

The formation of the main corrosion products can be explained as follows. At the early stage of corrosion, dezincification occurs because of the highly negative electrode potential of Zn:

$$Zn \rightarrow Zn^{2+} + 2e^- \quad (8)$$

The cathodic reaction mainly involves the reduction of H^+ (it was observed that some bubbles appeared on the surface of the tested samples at this stage):

$$2H^+ + 2e^- \rightarrow H_2 \uparrow \quad (9)$$

Observations showed that, after prolonged exposure to salt spray environment, the surface layer of the new alloy dealloyed and became dark. The corrosion of the alloy in this stage involves a series of reactions in the anodic and cathodic electrodes, mainly consisting of the oxidation of Cu and the reduction of O_2. The anodic reaction is:

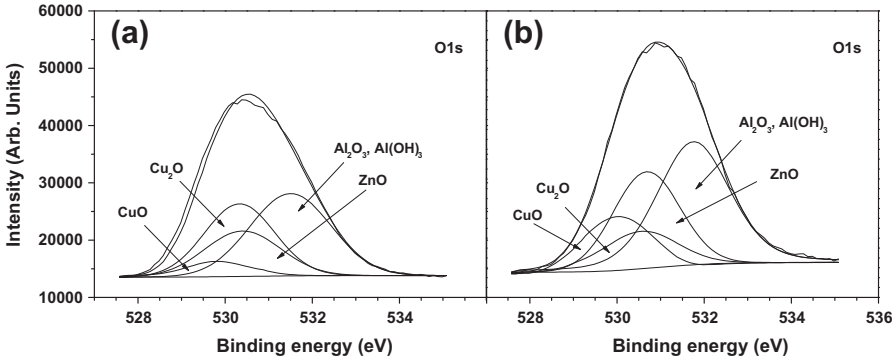

(c)

Valence state	*Exposure time (h)*	Proposed compounds	*Binding energy (eV)*	*Intensity area*	*Relative quantity*	$\Sigma\chi^2$
Al2p3/2	6	CuO	529.6	6751.74	0.076	1.38
		Cu_2O	530.3	31271.23	0.352	1.38
		ZnO	530.4	17323.55	0.195	1.38
		Al_2O_3/ $Al(OH)_3$	531.5	33492.2	0.377	1.38
	60	CuO	529.7	13468.2	0.107	1.21
		Cu_2O	530.4	18628.92	0.148	1.21
		ZnO	530.5	36628.47	0.291	1.21
		Al_2O_3/ $Al(OH)_3$	531.6	57145.43	0.454	1.21

Fig. 9. O XPS spectra and fitted parameters of the corrosion product layer of the samples exposed in salt spray environment for different times: (a) 6 h, (b) 60 h, and (c) fitting parameters for O XPS spectra and relative quantity of compounds.

$$Cu + Cl^- \rightarrow CuCl + e^- \quad (10)$$

followed by:

$$CuCl + Cl^- \rightarrow CuCl_2^- \quad (11)$$

The cathodic reaction is:

$$O_2 + 2H_2O + 4e^- \rightarrow 4OH^- \quad (12)$$

The CuCl formed during the corrosion process is easily dissolved and forms the cuprous complex $CuCl_2^-$ [25,26]. In the cases of high chloride concentrations, $CuCl_3^{2-}$ and $CuCl_4^{3-}$ may also be formed [25,27]. Subsequently, the cuprous oxide of Cu may be formed in the environment of OH^- through the reaction below:

$$2CuCl_2^- + 2OH^- \rightarrow Cu_2O + H_2O + 4Cl^- \quad (13)$$

Further oxidation of Cu, with the corrosion product of CuO, occurs with a prolonged exposure time under conditions of dissolved oxygen [28]. The stable Cu_2O could be oxidized to CuO through a sequence of reactions as follows [29]:

$$Cu_2O + O_2 + H_2O \rightarrow 2CuO + H_2O_2 \quad (14)$$

$$Cu_2O + H_2O_2 \rightarrow 2CuO + H_2O \quad (15)$$

Although $Cu(OH)_2$ and $Cu_2(OH)_3Cl$ can be produced by the hydrolysis of Cu_2O through the reactions [29]:

$$Cu_2O + 3H_2O \rightarrow 2Cu(OH)_2 + 2H^+ + 2e^- \quad (16)$$

$$Cu_2O + 2H_2O + Cl^- \rightarrow Cu_2(OH)_3Cl + H^+ \quad (17)$$

There is no evidence for the formation of these two corrosion products according to the XPS results of Cu2p3/2. Yuan et al. [17] investigated the corrosion products of a CuNi alloy in seawater environment for 10 days and also found no $Cu_2(OH)_3Cl$.

Al is oxidized during the corrosion process, with the anodic reaction of:

$$Al \rightarrow Al^{3+} + 3e \quad (18)$$

and cathodic reaction of:

$$2H^+ + 2e \rightarrow H_2 \uparrow \quad (19)$$

Because the salt spray solution is slightly alkaline due to the reduction of H^+, small amount of Al^{3+} can combine with OH^-:

$$Al^{3+} + 3OH^- \rightarrow Al(OH)_3 \downarrow \quad (20)$$

The precipitated aluminum hydroxide often forms gels and crystallizes with time. Al_2O_3 was formed in time by the following reaction:

$$Al(OH)_3 \rightarrow Al_2O_3 + H_2O \quad (21)$$

With prolonged corrosion time, the Al_2O_3 film becomes dense and should be effective to protect the alloy [4,30,31].

As discussed above, the corrosion products change from Cu_2O and ZnO in the early stage of corrosion to a mixture of CuO, Al_2O_3 and ZnO after prolonged exposure. A dense Al_2O_3 film protects the alloy from extensive corrosion.

3.5. Microstructure analysis

Fig. 10 shows the SEM images of the cross sections of the new and the H7211 alloys exposed in salt spray environment for 6 h and 60 h. It is obvious that the thickness of the oxide layer increased with exposure time. The corrosion product layer of the new alloy is uniform, with a thickness of 0.8 μm for 6 h exposure (Fig. 10a) and 4 μm for 60 h exposure (Fig 10b). The corrosion product layer of the H7211 alloy showed a typical intergranular

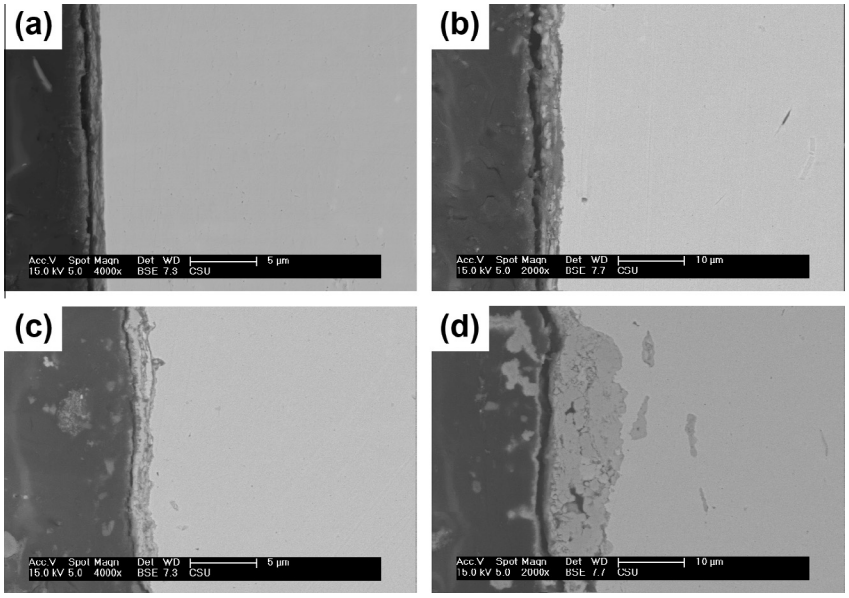

Fig. 10. SEM images of the cross sections of the samples exposed in salt spray environment for different times: (a) new alloy, 6 h; (b) new alloy, 60 h; (c) H7211, 6 h and (d) H7211, 60 h.

corrosion (Fig. 10c and d); its thickness is much greater than that of the new alloy for either exposure time.

It is well documented that the addition of aluminum to copper can improve its corrosion performance in sea water and salt solutions due to the formation of a sustainable protective layer of alumina (Al_2O_3) on the alloy surface [30,31]. The XPS analysis proved that Al_2O_3 existed in the corrosion product and its concentration increased with exposure time. It can be speculated based on these results that a protective layer of alumina formed during the corrosion process, which played an important role on the improvement of corrosion resistance of the new alloy.

The addition of B in the Al brass can not only refine the grains and strengthen the grain boundaries but also fill the vacancies, inhibiting the diffusion of Zn through these vacancies and resulting in improvement of the corrosion resistance [15,32]. Although dezincification is still observed in the new alloy, a great improvement has been made compared with the H7211 alloy.

Re is an active element and can easily be oxidized, leading to a small reduction in the corrosion resistance of the new alloy. However, Re can markedly improve the bonding of the corrosion product layer with the matrix, which can significantly increase the polarization resistance. In addition, Re is effective grain refiner and improves the mechanical properties of the alloy. The addition of less than 0.1% Re can also enhance the golden-color and improve the tarnish resistance [33].

4. Conclusions

(1) The newly-designed gold-imitation CuZnAlNiBCeSn alloy has better corrosion resistance and tarnish resistance than the H7211 alloy in salt spray environment. The polarization resistance R_p of the new alloy increased with exposure time in salt spray environment and was more than three times of that of the H7211 alloy for any given exposure time. The relationship between the color difference and corrosion time obeyed the power law in the early stage.

(2) EIS results showed that, with the extension of exposure time, the capacitance of the corrosion product film of the alloy, C_{film}, decreased, while the charge transfer resistance R_{ct}, Warburg diffusion impedance W_R and the resistance of the equivalent circuit R increased. The impedance spectra and the equivalent circuit analysis confirmed that a multi-layer film formed on the surface of the new alloy after a period of time in salt spray environment. This corrosion layer was responsible for the good corrosion resistance of the alloy.

(3) XPS results showed that the corrosion product layer formed on the alloy in salt spray environment mainly contained CuO, Cu_2O, ZnO, Al_2O_3 and $Al(OH)_3$, and there was no evidence for the existence of chloride. With increasing exposure time, there was a transition of the corrosion product from Cu_2O to CuO. The Al_2O_3 film protected the alloy from corrosion to some extent. The corrosion product layer of the new alloy is more uniform than that of the H7211 alloy.

Acknowledgements

The work was supported by two grants from the National Natural Science Foundation of China (51271203) and the Hunan Provincial Natural Science Foundation of China (11JJ2025).

References

[1] S. Sakai, S. Kaneko, K. Yajima, K. Kobayashi, Copper-based alloy, kitz corporation, EP, 1995.
[2] R. Ravichandran, S. Nanjundan, N. Rajendran, Corrosion inhibition of brass by benzotriazole derivatives in NaCl solution, Anti-Corrosion Methods and Materials 52 (2005) 226–232.
[3] T.-K.C.C.F. Mizoguchi, K.-K.C.C.F. Itoh, K.-K.C.C.F. Yajima, Copper-based alloy excellent in corrosion resistance, hot workability, and resistance to stress corrosion cracking, and process for producing the copper-based alloy, kitz corporation, EP, 2000.
[4] J.L. Chen, Z. Li, A.Y. Zhu, L.Y. Luo, J. Liang, Corrosion behavior of novel imitation-gold copper alloy with rare earth in 3.5% NaCl solution, Materials and Design 34 (2012) 618–623.
[5] G.R.S.B.C. Burrows, I.R.W.R. Scholes, Alloy for coins and the like, deleted IMI kynoch limited, EP, 1985.
[6] B.D. Prinz, M.B.D. Rockel, G.D. Rudolph, U.D. Heubner, H. Zoebe, Gold coloured alloy for coins, Vereinigte deutsche metallwerke AG, EP, 1982.
[7] J.Y. Song, S.I. Hong, Design and characterization of new Cu alloys to substitute Cu-25%Ni for coinage applications, Materials and Design 32 (2011) 1790–1795.
[8] U. Heubner, B. Prinz, M.B. Rockel, G. Rudolph, H. Zoebe, Gold coloured alloy for coins, 1982.
[9] S.S. Shilstein, S. Shalev, Making sense out of cents: compositional variations in European coins as a control model for archaeometallurgy, Journal of Archaeological Science 38 (2011) 1690–1698.

[10] B.Y. Huang, C.G. Li, L.K. Shi, G.Z. Qiu, T.Y. Zuo, China Materials Engineering Cannon, Chemistry Industry Press, Beijing, 2005.
[11] H. Gladen, H. Kaiser, H. Kaesche, A morphological study of dezincification of -brass, Corrosion Science 30 (1990) 737–741.
[12] L. Campanella, O.C. Alessandri, M. Ferretti, S.H. Plattner, The effect of tin on dezincification of archaeological copper alloys, Corrosion Science 51 (2009) 2183–2191.
[13] Z.I. Ortiz, P. Díaz-Arista, Y. Meas, R. Ortega-Borges, G. Trejo, Characterization of the corrosion products of electrodeposited Zn. Zn–Co and Zn–Mn alloys coatings, Corrosion Science 51 (2009) 2703–2715.
[14] C.D. Wanger, W.M. Riggs, L.E. Davis, J.F. Moulder, G.E. Mullenbery, Handbook of X-ray photoelectron spectroscopy, in: Physical Electronics Division, Perkin-Elmer Corporation, USA, 1979.
[15] C. Cao, Materials Corrosion in the Natural Environment in China, Chemistry Industry Press, Beijing, 2005.
[16] W.S. Tait, An introduction to electrochemical corrosion testing for practicing engineers and scientists, University of Wisconsin-Madison, Racine, USA, 1994.
[17] S.J. Yuan, S.O. Pehkonen, Surface characterization and corrosion behavior of 70/30 Cu–Ni alloy in pristine and sulfide-containing simulated seawater, Corrosion Science 49 (2007) 1276–1304.
[18] X. Zhang, S.O. Pehkonen, N. Kocherginsky, G.A. Ellis, Copper corrosion in mildly alkaline water with the disinfectant monochloramine, Corrosion Science 44 (2002) 2507–2528.
[19] P. Druska, H.H. Strehblow, S. Golledge, Surface analytical examination of passive layers on Cu/Ni alloys: Part I. Alkaline solution, Corrosion Science 38 (1996) 835–851.
[20] M. Lebrini, G. Fontaine, L. Gengembre, M. Traisnel, O. Lerasle, N. Genet, Corrosion behaviour of galvanized steel and electroplating steel in aqueous solution: AC impedance study and XPS, Applied Surface Science 254 (2008) 6943–6947.
[21] R. Procaccini, M. Vazquez, S. Cere, Copper and brass aged at open circuit potential in slightly alkaline solutions, Electrochimica Acta 54 (2009) 7324–7329.
[22] B.A. Boukamp, A nonlinear least squares fit procedure for analysis of immittance data of electrochemical systems, Solid State Ionics, Diffusion and Amp Reactions 20 (1986) 31–44.
[23] M.A. Amin, K.F. Khaled, Copper corrosion inhibition in O_2-saturated H_2SO_4 solutions, Corrosion Science 52 (2010) 1194–1204.
[24] L.E. Eiselstein, B.C. Syrett, S.S. Wing, R.D. Caligiuri, The accelerated corrosion of CuNi alloys in sulphide-polluted seawater: mechanism no. 2, Corrosion Science 23 (1983) 223–239.
[25] S. Hong, W. Chen, H. Luo, N. Li, Inhibition effect of 4-amino-antipyrine on the corrosion of copper in 3 wt.%NaCl solution, Corrosion Science 57 (2012) 270–278.
[26] S. Hong, W. Chen, Y. Zhang, H. Luo, M. Li, N. Li, Investigation of the inhibition effect of trithiocyanuric acid on corrosion of copper in 3.0 wt.% NaCl, Corrosion Science 66 (2013) 308–314.
[27] W.A. Badawy, K.M. Ismail, A.M. Fathi, Effect of Ni content on the corrosion behavior of Cu–Ni alloys in neutral chloride solutions, Electrochimica Acta 50 (2005) 3603–3608.
[28] S. Campbell, F.C. Walsh, N. Campbell, E.B.G. Jones, Developments in Marine Corrosion, Royal Society of Chemistry, Cambridge, 1998.
[29] S.R. de Sanchez, L.E.A. Berlouis, D.J. Schiffrin, Difference reflectance spectroscopy of anodic films on copper and copper base alloys, Journal of Electroanalytical Chemistry and Interfacial Electrochemistry 307 (1991). 73-73.
[30] A. Schussler, H.E. Exner, The corrosion of nickel–aluminium bronzes in seawater I. Protective layer formation and the passivation mechanism, Corrosion Science 34 (1993) 1793–1802.
[31] A. Schussler, H.E. Exner, The corrosion of nickel–aluminium bronzes in seawater-II. The corrosion mechanism in the presence of sulphide pollution, Corrosion Science 34 (1993) 1803–1815.
[32] V.F. Lucey, The mechanism of dezincification and the effect of arsenic, British Corrosion Journal 1 (1965) 9–14.
[33] D. Tang, Z. Zhou, J. Ge, A study of the colour-stable alloy imitation gold, Metal Science and Technology 10 (1991) 77–82.